6 Selection of the optimal pulse sequence for functional MRI

Peter A. Bandettini

6.1 Introduction

Since its inception in 1991, functional MRI (fMRI) has experienced an explosive growth in the number of users and a steady widening in its range of applications. A recent (2000) search of the National Library of Medicine database for articles with 'fMRI' or 'BOLD' in the title revealed over 1000 citations. The rapid rate of improvement in pulse sequence design, data processing, information content, data interpretation, and paradigm design can be overwhelming to the novice and even to the advanced user. This chapter is written to assist the fMRI user in making an informed decision regarding the choice of functional MRI pulse sequence. A second goal is to present the pulse sequence choices against a wider backdrop of relevant variables, ranging from paradigm timing to available hardware. The hope is to build a broader perspective of what the limits and possibilities of fMRI are.

Most fMRI experimental planning can be reduced to an iterative optimization between what is practically possible and what is ideally desired from the experiment—both factors being inter-dependent. They drive both the development of the methodology and the sophistication of the questions that can be asked. The following sections describe the variables that can be optimized in typical functional MRI experiments. These factors include information content, sensitivity, acquisition speed, image resolution, brain coverage, and anatomical image quality. Summaries and discussions of the tradeoffs regarding the variables described are included.

6.2 Information content

Several types of physiological information can be mapped using fMRI. This range of information includes the following: baseline cerebral blood volume (Rosen *et al.* 1989; Moonen *et al.* 1990; Rosen *et al.* 1991), changes in blood volume (Belliveau *et al.* 1991), baseline and changes in cerebral perfusion (Detre *et al.* 1992; Williams *et al.* 1992; Edelman *et al.* 1994*b*; Kwong *et al.* 1994; Kim 1995; Wong *et al.* 1997), and changes in blood oxygenation (Ogawa *et al.* 1990; Turner *et al.* 1991; Bandettini *et al.* 1992; Frahm *et al.* 1992; Kwong *et al.* 1992; Ogawa and Lee 1992; Haacke *et al.* 1997). Recent advances in fMRI pulse sequence and experimental manipulation have allowed quantitative measures of oxygen metabolism ($CMRO_2$) changes and dynamic non-invasive measures in blood volume with activation to be extracted from fMRI data (Kim and Ugurbil 1997; Davis *et al.* 1998; van Zijl *et al.* 1998; Hoge *et al.* 1999*a*,*b*). A detailed treatment of the MRI techniques available to map these physiological parameters, in particular $CMRO_2$ estimation, is provided in Chapter 8. Table 6.1 provides a summary of the tradeoffs involved with the use of each of the above mentioned contrast mechanisms and the types of information that can be obtained from each. Also, a brief overview of the basic principles is given below.

6.2.1 Blood volume

In the late 1980s, the use of rapid MRI allowed tracking of transient signal intensity changes over time. One application of this utility was to follow the T2* or T2-weighted signal intensity changes as a bolus of intravascular paramagnetic contrast agent passed through the tissue of interest (Rosen *et al.* 1989). As it passes through, the bolus induces susceptibility-related signal dephasing which then recovers as the bolus washes out. The area under the signal attenuation curve is proportional to the relative blood volume. In 1990, Belliveau and colleagues took this approach one

Table 6.1 Summary of the practical advantages and disadvantages of pulse sequences that have contrast based on BOLD, perfusion, volume, and $CMRO_2$

	Advantages	Disadvantages
BOLD	• highest functional activation contrast by a factor of 2 to 4 over perfusion • easiest to implement • multislice trivial • can use very short TR	• complicated non-quantitative signal • no baseline information • susceptibility artefacts
Perfusion	• unique and quantitative information • baseline information • easy control over observed vasculature • non-invasive • no susceptibility artefacts	• low functional activation contrast • longer TR required • multislice is difficult • slow mapping of baseline information
Volume	• unique information • baseline information • multislice is trivial • rapid mapping of baseline information	• invasive • susceptibility artefacts • requires separate rest and activation runs
$CMRO_2$	• unique and quantitative information	• semi-invasive • extremely low functional activation contrast • susceptibility artefacts • processing intensive • multislice is difficult • longer TR required

step further when they mapped blood volume during rest and during activation (Belliveau *et al.* 1991). Indeed, the first maps of brain activation using fMRI were demonstrated with this technique. Soon after its demonstration, contrast agent fMRI was rendered largely obsolete (for brain activation imaging) by the endogenous oxygen-sensitive contrast agent haemoglobin. Recently, non-invasive methods for dynamic measurement of blood volume have been introduced (Liu *et al.* 2000).

One advantage of blood volume mapping is that the information that is derived is directly interpretable, and that baseline information on blood volume and perfusion (which can be derived by taking into consideration the measured tissue transit time) can be obtained. It also has the advantage that multi-slice imaging is trivial and a very short scan repeat time (TR) can be used, if desired. The total time required for the acquisition of data required for a blood volume measurement is also quite short (approximately 2 min).

Blood volume mapping with a bolus injection of a susceptibility contrast agent has its drawbacks, however. Even though the contrast agents are non-toxic at the doses given, the technique is considered invasive. Larger doses or repeated doses would become toxic. All brain activation maps obtained with this technique involve separate runs of about 2 min each: the first being a rest state, and the second an activated state. Since the number of repeated doses is limited, a constraint is placed on what types of cognitive question can be asked with the use of this technique. Because of the limited number of brain activation studies that have been performed with this technique, it is difficult to draw a conclusion regarding the relative contrast-to-noise ratio provided by its functional activation maps.

6.2.2 Blood oxygenation

As early as the 1930s it was known that deoxyhaemoglobin was paramagnetic and oxyhaemoglobin was diamagnetic (Pauling and Coryell 1936). In 1982 it was discovered that decreases in blood oxygenation lead to a decrease in the T2 NMR relaxation time of blood (Thulborn *et al.* 1982), and also lead to

decreases in T2*. It was not until 1989 that this knowledge was used to image *in vivo* changes in blood oxygenation in rat. Blood oxygenation level dependent contrast, coined BOLD by Ogawa (Ogawa *et al.* 1992), was used to image the activated human brain for the first time in 1991, and the first results using BOLD contrast for imaging brain function were published in 1992 (Bandettini *et al.* 1992; Kwong *et al.* 1992; Ogawa *et al.* 1992). The basic concept behind this contrast mechanism is described in detail elsewhere in this book. The effect of neuronal activity is to produce an increase in T2 and T2*, and thus to cause a small signal increase in T2 and T2*-weighted images. Because of its improved sensitivity and ease of implementation, gradient echo (T2*-weighted) BOLD imaging has emerged as being the most commonly used fMRI method. Asymmetric spin echo techniques, used extensively by one of the first groups to perform fMRI (Kwong *et al.* 1992), have similar contrast as gradient echo techniques and have been implemented with similar results.

With BOLD contrast, several distinct advantages exist. First, the technique is of course completely non-invasive. Second, the functional contrast-to-noise ratio is at least a factor of 2 to 4 greater than that of perfusion imaging (i.e. the functional maps are much less noisy). Third, it is easiest to implement since it only requires, typically, a gradient echo sequence with an echo time (TE) of 30 to 40 ms. Fourth, it is trivial to perform multi-slice whole brain echo planar imaging (EPI). All that is required is that the repetition time (TR) be long enough to accommodate all of the slices desired in each volume. Typically, with a TE of about 40 ms, the total time for acquiring a single-shot echo planar image is about 60 to 100 ms, which translates to a maximum rate of 10 to 16 slices per second. If a reduced number of slices is sufficient, then a very short TR can be utilized for fine temporal mapping of the dynamics of the BOLD signal change, though the signal-to-noise ratio can be compromised under such conditions due to incomplete T1 recovery of magetisation between subsequent slice excitations.

Despite some clear advantages, several disadvantages do, however, exist in regard to BOLD contrast imaging. First, as is described in Chapters 2 and 8, the physiology underlying BOLD contrast is extremely complicated, involving the interplay of perfusion, $CMRO_2$, and blood volume changes, and is further modulated by the heterogeneity of the vasculature and neuro-vascular coupling over time and space. This problem leads to limits of interpretation in the location, magnitude, linearity, and dynamics of the BOLD contrast signal. In addition, it makes comparisons over populations, clinical mapping, and mapping of the effects of pharmacologic intervention extremely challenging. Also, unlike the perfusion and volume mapping methods, no baseline oxygenation information can, as yet, be obtained since resting state T2* and T2 times are dominated by the type of tissue rather than by its oxygenation state. If resting state oxygenation information is required, considerable assumptions have to be made regarding blood volume and vessel geometry, among other things. Another problem with BOLD contrast in general is that the same susceptibility weighting that allows for the observation of the functional contrast also contributes to many of the artefacts in the images used. These artefacts include signal dropout at tissue interfaces and at the base of the brain. This problem becomes greater at higher field strengths.

6.2.3 Blood perfusion

An array of new techniques exists for mapping cerebral blood *perfusion* in humans. For a recent review, please refer to Wong (1999). Perfusion MRI techniques based on arterial spin labeling, abbreviated as ASL techniques, are conceptually similar to other modalities such as positron emission tomography (PET) and single photon emission computed tomography (SPECT) in that they involve tagging of inflowing blood, and then allow flow of the tagged blood into the imaging plane. In MRI a radiofrequency (RF) tagging pulse is used, which is usually a 180° pulse that 'inverts' the arterial blood magnetization.

ASL techniques can be subdivided into those that use continuous arterial spin labeling, which involves continuously inverting arterial blood flowing into the slice of interest, and those that use pulsed arterial spin labeling, which involves periodically inverting a 'plug' of arterial blood and measuring the arrival of that blood into the imaging slice. Examples of these techniques include 'echo planar imaging with signal targeting and alternating RF' (EPISTAR) (Edelman *et al.* 1994*a*) and 'flow-sensitive alternating inversion recovery' (FAIR) (Kim 1995; Kwong *et al.* 1995).

Recently, a pulsed arterial spin labeling technique known as 'quantitative imaging of perfusion using a single subtraction' (QUIPSS), has been introduced (Wong *et al.* 1998).

The primary advantage of perfusion mapping is that quantitative maps of perfusion changes can be obtained, at least in principle. The changes in signal are simply due to perfusion effects and not based on any complicating interactions of neurovascular coupling and blood volume dynamics. Also, quantitative maps of resting state or baseline perfusion are obtained by default in every time series. With modulation of the timing parameters such as the inversion time (TI) specific parts of the vasculature may be isolated based on their flow rates. Since the tagging of inflowing spins involves only the use of an RF pulse, the technique is non-invasive. Lastly, since the basis of the contrast is not susceptibility, an extremely short TE can be used, significantly reducing larger scale susceptibility artefacts. For this reason, this technique might be the method of choice for mapping activation near the problematic tissue interfaces and at the base of the brain.

Perfusion imaging has several potentially prohibitive disadvantages, however. First, the functional contrast-to-noise ratio is lower than BOLD contrast by a factor of about 2 to 4, leading to the requirement of more temporal averaging (by a factor of 4 to 16) to achieve similar quality activation maps. Second, because of the time (TI) required to allow the tagged blood to perfuse into the tissue of interest, a relatively long TR is required. The minimum TR that can be used is typically 2 s. Nevertheless, techniques are emerging that allow for a shorter TR to be used (Liu and Gao1999; Duyn *et al.* 2000; Wong *et al.* 2000*b*) or that provide other solutions (Buxton *et al.* 1998*a*,*b*) by using periodically divisible TR and stimulus timing intervals. Third, because the tagged blood spins undergo signal decay from the moment they are tagged (dictated by the T1 of blood), all the images have to be acquired in a very short time, putting a limit on the number of slices that can be obtained. Under such multi slice conditions, each slice also has a different TI associated with it, making quantification slightly more difficult. The typical upper limit of slices is in the range of 5 to 10. Finally, in a clinical setting where mapping of baseline perfusion information may be critical, ASL requires more scanning time to create a usable perfusion map than does the currently used method involving dynamic imaging following the injection of a bolus of contrast agent. Although such contrast injection methods are better able to measure relative blood volume, perfusion maps can also be obtained if the tissue transit times are available.

For mapping baseline information, ASL is slower than such dynamic contrast agent methods by a factor of at least 3, which is potentially critical when determining compromised perfusion in acute stroke, for instance.

6.2.4 Haemodynamic specificity

Each of the MRI techniques outlined above relies on the ^{1}H nuclei within water molecules to provide its signal. These water spins are in a number of vascular and tissue environments and, depending on the details of the MRI pulse sequence used, each environment may contribute more or less of the signal. Importantly, a poor choice of sequence parameters may introduce signals from unwanted environments that may affect

Fig. 6.1 The vascular tree, including (*left to right*) arteries, arterioles, capillaries, venules, and veins. The figures illustrate the signal seen from the vessels and from surrounding tissue for different classes of MRI pulse sequence. In the case of arterial spin labeled perfusion sequences (a) signal is detected from the water spins in the arterial–capillary region of the vasculature and from water in tissue surrounding the capillaries. The relative sensitivity of these contributions can be controlled by adjusting the TI inversion time and by incorporation of velocity nulling (also known as diffusion weighting) gradients. A small amount of velocity nulling and a TI of approx. 1 s makes ASL perfusion techniques selectively sensitive to capillaries and tissue and less sensitive to large vessel effects (*lower figure*). Gradient echo BOLD techniques (b) are sensitive to susceptibility perturbers of all sizes, and are therefore sensitive to all intravascular and extravascular effects in the capillary-venous portion of the vasculature. Spin echo BOLD techniques (c) are sensitive to susceptibility perturbers about the size of a red blood cell or capillary, making them predominantly sensitive to intravascular water spins in vessels of all sizes and to extravascular (tissue) water surrounding capillaries. Use of velocity nulling gradients reduces the contribution of signal from larger vessels (venules and veins). If a very short TR scan repeat time is used, then GE-BOLD methods may additionally show signal originating from arterial inflow, which can be removed by using a longer TR and/or outer volume saturation.

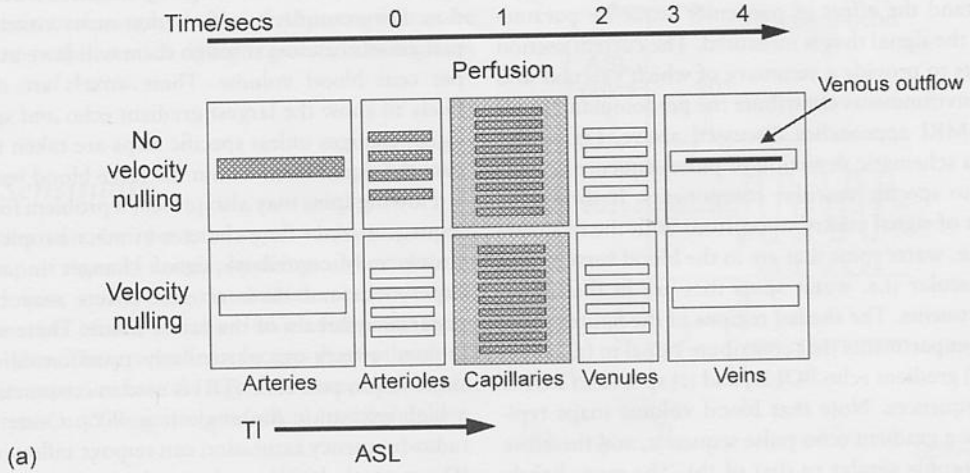
Time/secs
0
1
2
3
4
Perfusion
Venous outflow
No velocity nulling
Velocity nulling
Arteries
Arterioles
Capillaries
Venules
Veins
TI
ASL

(a)

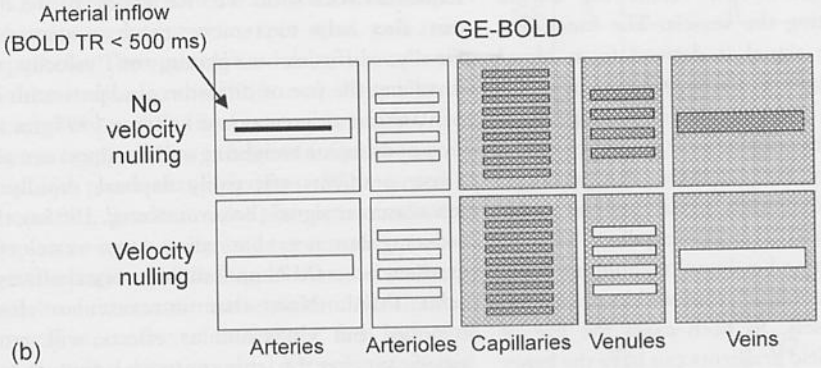
Arterial inflow
(BOLD TR < 500 ms)
GE-BOLD
No velocity nulling
Velocity nulling
Arteries
Arterioles
Capillaries
Venules
Veins

(b)

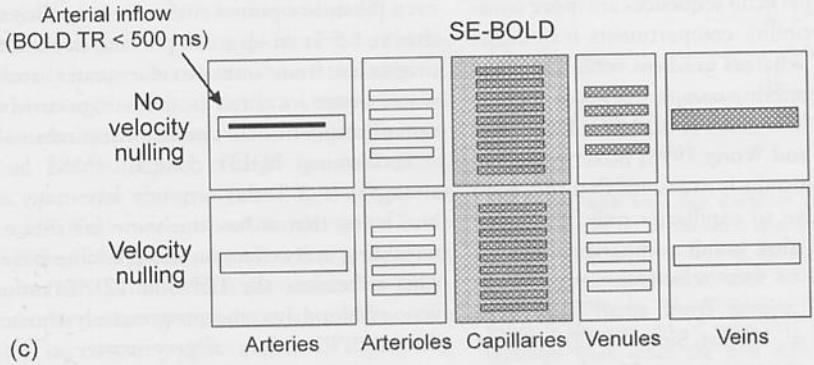
Arterial inflow
(BOLD TR < 500 ms)
SE-BOLD
No velocity nulling
Velocity nulling
Arteries
Arterioles
Capillaries
Venules
Veins

(c)

the interpretation of the data. It is, therefore, crucial to understand the effect of particular sequence parameters on the signal that is measured. The current section attempts to provide a summary of which vascular and tissue environments contribute the predominant signal to the MRI approaches discussed above. Figure 6.1 shows a schematic depiction of pulse sequence sensitization to specific vascular components. It shows the amount of signal contribution from both the intravascular (i.e. water spins that are in the blood vessels) and extravascular (i.e. water spins that are in the tissue) compartments. The shaded regions of the figures show those compartments that contribute signal to (a) perfusion, (b) gradient echo BOLD, and (c) spin echo BOLD pulse sequences. Note that blood volume maps typically use a gradient echo pulse sequence, and therefore have a profile similar to that of (b). The more lightly shaded regions surrounding the vessels depict extravascular (tissue) contributions, versus the darker shaded regions depicting the vessels. The functional contrast in the tissue signal is derived from blood water spins exchanging with tissue water spins in the case of ASL perfusion, and from spin dephasing effects (in the presence of extravascular field gradients) in the case of BOLD. Broadly, Fig. 6.1 shows that perfusion techniques show predominantly signal contrast either from within or around arterial—capillary vessels, whereas BOLD (and blood volume) techniques show predominantly signal contrast from within or around capillary—venous vessels. In both cases the use of some velocity nulling field gradients can have the beneficial effect of minimizing unwanted signal changes from within the very large vessels.

Regarding susceptibility contrast (BOLD) imaging, Fig. 6.1 shows that spin echo sequences are more sensitive to small susceptibility compartments (capillaries and red blood cells) whereas gradient echo sequences are sensitive to susceptibility compartments of all sizes (Ogawa *et al.* 1993; Weisskoff *et al.* 1993; Kennan *et al.* 1994; Bandettini and Wong 1995; Boxerman *et al.* 1995*b*). A common mistake is to assume that spin echo sequences are sensitive to capillaries only. Since red blood cells also are also 'small compartments' spin echo sequences are in fact selectively sensitive to intravascular signal arising from small *and* large vessels (Boxerman *et al.* 1995*a*). Since BOLD contrast is highly weighted by the resting state blood volume in the voxel it is important to consider the vascular content of voxels showing significant BOLD activation. For example, it is likely that many voxels having pial vessels running through them will have at least 50 per cent blood volume. These voxels are therefore likely to show the largest gradient echo *and* spin echo signal changes unless specific steps are taken to eliminate the signal from within the large blood vessels.

Flowing spins may also present a problem for BOLD sequences, since flow changes in macroscopic arterial vessels may contribute signal changes in an fMRI experiment and these arterial effects may be some distance upstream of the active tissue. These so called 'inflow' effects are particularly pronounced when a short scan repeat time (TR) is used in conjunction with a high excitation flip angle (e.g. 90°). Outer volume radio-frequency saturation can remove inflowing spins (Duyn *et al.* 1994), and can thus reduce such non-susceptibility related inflow changes when using sequences with short TR. Reduction of the flip angle can also help to remove these unwanted effects. Finally, diffusion weighting, or 'velocity nulling', involving the use of diffusion gradients with b-values of 50 s^2/mm or greater (see LeBihan 1995, for a discussion of diffusion weighting and b-values) can also help. These gradients effectively dephase rapidly moving intravascular signal (Boxerman *et al.* 1995*a*), therefore reducing but not eliminating large vessel effects in gradient echo fMRI and all large vessel effects in spin echo fMRI. Note that intravascular effects are removed but extravascular effects will remain. A significant caveat to this approach is that, at 1.5 Tesla, application of this amount of diffusion weighting reduces the BOLD signal change by about 60 per cent (Boxerman *et al.* 1995*a*) which is prohibitive under even the most optimal circumstances. This also implies that at 1.5 Tesla up to 60 per cent of the BOLD signal originates from intravascular water and not from water better localized in tissue experiencing modulation of magnetic field gradients around smaller vessels.

Performing BOLD contrast fMRI at high field strengths (> 3 Tesla) certainly has many advantages, one being that it has the same benefits as diffusion weighting in its effect on susceptibility-based contrast. This is because the T2* and T2 relaxation times of venous blood become progressively shorter than the T2* and T2 values of grey matter as a function of increasing static field strength. Therefore, proportionately less signal will arise from intravascular water at

the interpretation of the data. It is, therefore, crucial to understand the effect of particular sequence parameters on the signal that is measured. The current section attempts to provide a summary of which vascular and tissue environments contribute the predominant signal to the MRI approaches discussed above. Figure 6.1 shows a schematic depiction of pulse sequence sensitization to specific vascular components. It shows the amount of signal contribution from both the intravascular (i.e. water spins that are in the blood vessels) and extravascular (i.e. water spins that are in the tissue) compartments. The shaded regions of the figures show those compartments that contribute signal to (a) perfusion, (b) gradient echo BOLD, and (c) spin echo BOLD pulse sequences. Note that blood volume maps typically use a gradient echo pulse sequence, and therefore have a profile similar to that of (b). The more lightly shaded regions surrounding the vessels depict extravascular (tissue) contributions, versus the darker shaded regions depicting the vessels. The functional contrast in the tissue signal is derived from blood water spins exchanging with tissue water spins in the case of ASL perfusion, and from spin dephasing effects (in the presence of extravascular field gradients) in the case of BOLD. Broadly, Fig. 6.1 shows that perfusion techniques show predominantly signal contrast either from within or around arterial—capillary vessels, whereas BOLD (and blood volume) techniques show predominantly signal contrast from within or around capillary—venous vessels. In both cases the use of some velocity nulling field gradients can have the beneficial effect of minimizing unwanted signal changes from within the very large vessels.

Regarding susceptibility contrast (BOLD) imaging, Fig. 6.1 shows that spin echo sequences are more sensitive to small susceptibility compartments (capillaries and red blood cells) whereas gradient echo sequences are sensitive to susceptibility compartments of all sizes (Ogawa *et al.* 1993; Weisskoff *et al.* 1993; Kennan *et al.* 1994; Bandettini and Wong 1995; Boxerman *et al.* 1995*b*). A common mistake is to assume that spin echo sequences are sensitive to capillaries only. Since red blood cells also are also 'small compartments' spin echo sequences are in fact selectively sensitive to intravascular signal arising from small *and* large vessels (Boxerman *et al.* 1995*a*). Since BOLD contrast is highly weighted by the resting state blood volume in the voxel it is important to consider the vascular content of voxels showing significant BOLD activation. For example, it is likely that many voxels having pial vessels running through them will have at least 50 per cent blood volume. These voxels are therefore likely to show the largest gradient echo *and* spin echo signal changes unless specific steps are taken to eliminate the signal from within the large blood vessels.

Flowing spins may also present a problem for BOLD sequences, since flow changes in macroscopic arterial vessels may contribute signal changes in an fMRI experiment and these arterial effects may be some distance upstream of the active tissue. These so called 'inflow' effects are particularly pronounced when a short scan repeat time (TR) is used in conjunction with a high excitation flip angle (e.g. 90°). Outer volume radio-frequency saturation can remove inflowing spins (Duyn *et al.* 1994), and can thus reduce such non-susceptibility related inflow changes when using sequences with short TR. Reduction of the flip angle can also help to remove these unwanted effects. Finally, diffusion weighting, or 'velocity nulling', involving the use of diffusion gradients with b-values of 50 s^2/mm or greater (see LeBihan 1995, for a discussion of diffusion weighting and b-values) can also help. These gradients effectively dephase rapidly moving intravascular signal (Boxerman *et al.* 1995*a*), therefore reducing but not eliminating large vessel effects in gradient echo fMRI and all large vessel effects in spin echo fMRI. Note that intravascular effects are removed but extravascular effects will remain. A significant caveat to this approach is that, at 1.5 Tesla, application of this amount of diffusion weighting reduces the BOLD signal change by about 60 per cent (Boxerman *et al.* 1995*a*) which is prohibitive under even the most optimal circumstances. This also implies that at 1.5 Tesla up to 60 per cent of the BOLD signal originates from intravascular water and not from water better localized in tissue experiencing modulation of magnetic field gradients around smaller vessels.

Performing BOLD contrast fMRI at high field strengths (> 3 Tesla) certainly has many advantages, one being that it has the same benefits as diffusion weighting in its effect on susceptibility-based contrast. This is because the T2* and T2 relaxation times of venous blood become progressively shorter than the T2* and T2 values of grey matter as a function of increasing static field strength. Therefore, proportionately less signal will arise from intravascular water at

Table 6.2 Approximated values for grey matter relaxation times and activation-induced relaxation rate changes. These values are used specifically for the illustration of contrast and per cent change curves in Figure 6.3

	1.5T	3T
T2	100 ms	80 ms
T2*	60 ms	50 ms
T2′	150 ms	133.3 ms
$\Delta R2 = \Delta(1/T2)$	$-0.2\ s^{-1}$	$-0.4\ s^{-1}$
$\Delta R2^* = \Delta(1/T2^*)$	$-0.8\ s^{-1}$	$-1.6\ s^{-1}$
$\Delta R2' = \Delta(1/T2')$	$-0.6\ s^{-1}$	$-1.2\ s^{-1}$

in T2 rather than T2* are observed, the optimal TE ≈ resting T2. Note from Fig. 6.3 that the percentage signal change increases linearly with TE while the contrast has a well defined peak.

In the case of the asymmetric spin echo sequence, BOLD contrast is generated when the image is collected at a time, τ, from the spin echo. To maximize BOLD contrast, τ should also be approximately equal to the T2* of the tissue.

For arterial spin labeling sequences the basic EPI readout module is still used, but an ASL tagging pulse is added a time TI before the EPI readout. It is desirable to tailor the pulse sequence parameters such that the perfusion maps show only tissue perfusion with no signal seen in larger arteries from tagged blood that is destined for more distal slices. This can be accomplished by careful choice of tagging pulse parameters and by use of flow-crushing gradient pulses. The rationale is to optimize quantification or information content (Wong *et al.* 1998; Wong 1999). If full control for quantification is not necessary, and some contamination from blood which is flowing through the slice is acceptable, then maps having greater functional contrast by at least a factor of 2 can be obtained by relaxing some of the above constraints.

While not directly improving perfusion contrast itself, one simple method for improving ASL signal-to-noise ratio without compromising quantification is the use of as short a TE as possible. For example, in single shot-imaging, starting at the centre of *k*-space, as with spiral imaging, allows for an extremely short TE (as short as 3 ms), yielding higher signal-to-noise ratio in the raw images.

Methods exist that are able to collect both BOLD contrast and perfusion contrast in a single experimental run. These include techniques that collect perfusion images and BOLD images during separate segments of the same run (Hoge *et al.* 1999*a*), those that use the same images for perfusion and BOLD contrast calculations (Wong and Bandettini 1999), and those that employ a double echo sequence—using the first echo (short TE: no T2*-weighting) for optimally obtaining perfusion information and the second echo (long TE: high T2*-weighting) for optimally obtaining BOLD information.

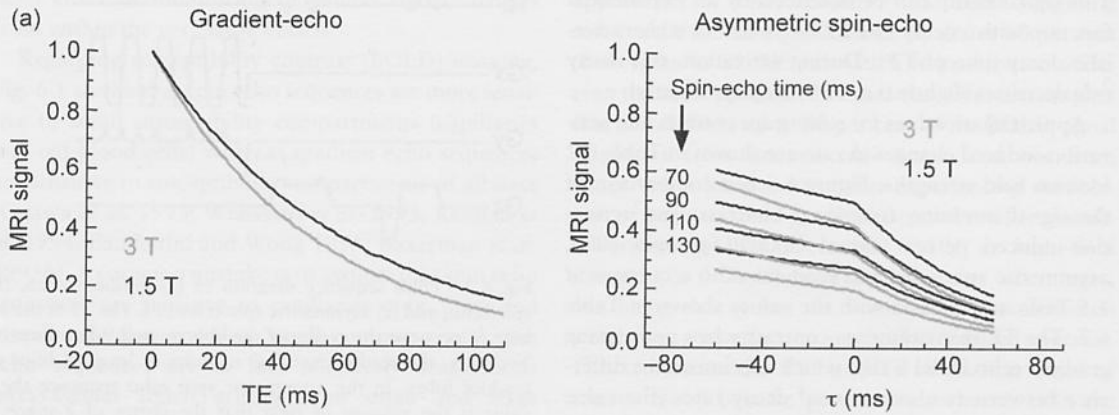

Fig. 6.3 (a) Comparison of signal intensity for gradient echo, asymmetric spin echo, and spin echo sequences for approximated decay rates of grey matter for 1.5 Tesla and 3 Tesla. The values from Table 6.2 were used. Note that the spin echo sequence corresponds to $\tau = 0$.

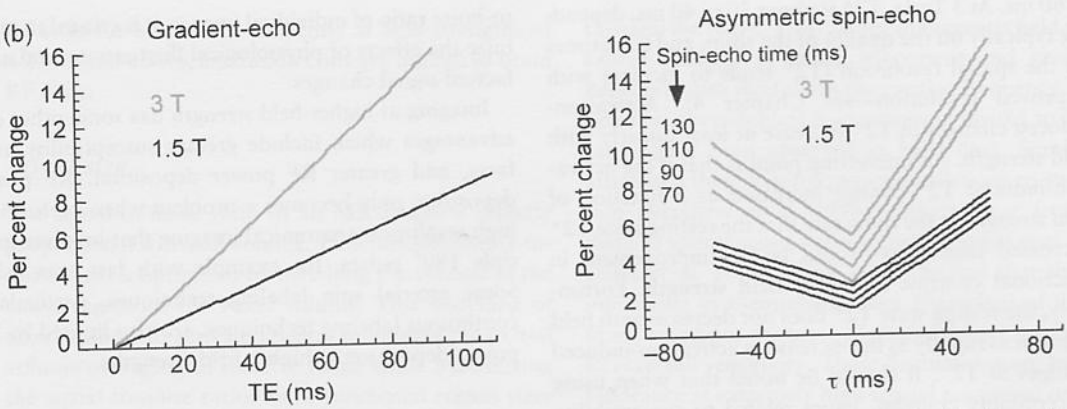

Fig. 6.3 (b) Comparison of the percent signal change with brain activation for gradient echo, asymmetric spin echo, and spin echo sequences for approximated activation-induced relaxation rate changes for 1.5 Tesla and 3 Tesla (taken from Table 6.2). With gradient echo sequences and with increasing τ for the asymmetric spin echo sequence, and for the spin echo ($\tau = 0$) the percent signal change has an approximately linear relationship with TE.

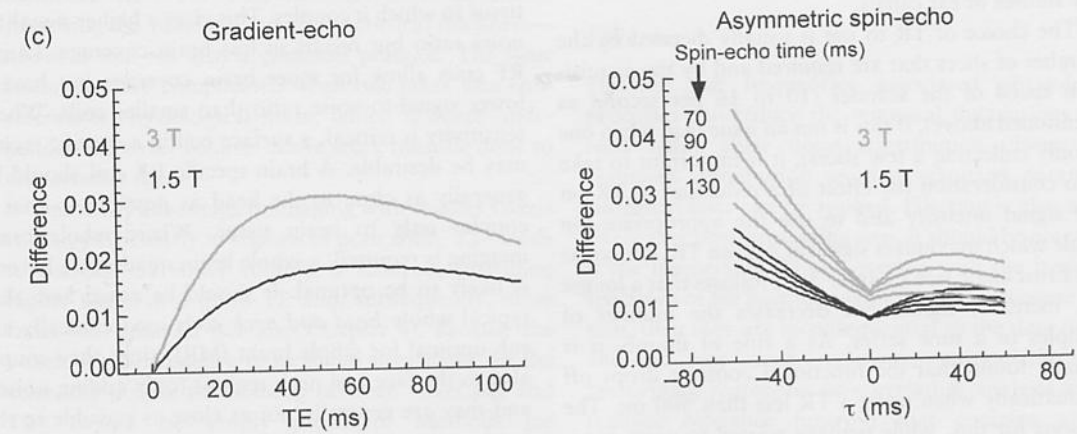

Fig. 6.3 (c) Comparison of the signal difference or contrast with brain activation for gradient echo, asymmetric spin echo, and spin echo sequences for approximated activation-induced relaxation rate changes for 1.5 Tesla and 3 Tesla (taken from Table 6.2). Note that there is a peak in contrast for gradient echo sequences at TE ≈ T2* and with asymmetric spin echo sequences for $\tau \approx$ T2*. Also note that spin echo sequences ($\tau = 0$) have the lowest contrast.

6.3.2 Maximizing signal

Field strength and sequence parameters

Imaging at higher static field strength increases both the anatomical image signal-to-noise ratio and also the magnitude of the activation-induced signal change for BOLD and perfusion contrast (Menon *et al.* 1993; Ugurbil *et al.*, 1993). MRI signal-to-noise ratio increases linearly with field strength because the net magnetization (or proton magnetic moment) increases in proportion to field strength. BOLD contrast calculations are slightly more complicated (Moonen and van Gelderen 1999). The magnitude of the BOLD signal change increases in a manner that is approximately linear with field strength due to a greater stratification in precession frequencies for a given change in blood oxygenation. Regarding functional *contrast*, BOLD contrast, as mentioned above, is maximized with TE ≈ T2* of grey matter. At 1.5 Tesla, T2* is about 50

to 60 ms. At 3 Tesla, T2* is about 30 to 40 ms, depending typically on the quality of the shim, and sometimes on the spatial resolution (T2* tends to increase with improved resolution—see Chapter 4). Activation-induced changes in T2* increase at least linearly with field strength. An interesting point is that if the activation-induced T2* change increased as a function of field strength at the same rate that the resting state T2* decreased then there would be no improvement in functional contrast at higher field strength. Fortunately, the resting state T2* does not decrease with field strength as rapidly as the increase in activation-induced changes in T2*. It should be noted that when using susceptibility contrast, issues related to susceptibility problems, such as shimming and distortion, are more prominent at higher field strengths. This becomes most significant when imaging the base of the brain or regions near interfaces of susceptibility, such as near the sinuses or ear canals.

The choice of TR to use is usually dictated by the number of slices that are required and by the acquisition speed of the scanner (10 to 16 per second as mentioned above). If this is not an issue (e.g. when one is only collecting a few slices), it is important to take into consideration the effect of a reduction in TR on the signal intensity and to use the appropriate flip angle which maximizes signal at a given TR, known as the Ernst angle (see Chapter 3). It follows that a longer TR increases signal, but decreases the number of samples in a time series. As a rule of thumb, it is usually found that the functional contrast drops off dramatically when using a TR less than 500 ms. The reasons for this, while perhaps related to noise autocorrelation, are as yet somewhat unclear.

When performing arterial spin labeling, functional perfusion contrast also increases at higher field strengths. The T1 or longitudinal relaxation time of blood increases with field strength, resulting in more signal from the tagged inflowing blood.

An important point discussed in Section 6.3.3 is that an increase in image signal-to-noise ratio or functional contrast does not necessarily translate to higher functional contrast-to-noise ratio since functional images are created from time series data. Noise in time series data contains physiological fluctuations as well as artefactual signal changes which reduce the quality of the functional images (Jezzard 1999). To reap the full benefits from increasing the signal intensity and signal-to-noise ratio of individual images, it is critical to minimize the effects of physiological fluctuations and artefactual signal changes.

Imaging at higher field strength has some other disadvantages which include greater susceptibility artefacts, and greater RF power deposition. RF power deposition only becomes a problem when performing high resolution anatomical imaging that involves multiple 180° pulses, for example with fast spin echo. Some arterial spin labeling techniques, particularly continuous labeling techniques, are also limited by RF power deposition at higher field strengths.

Radio frequency coils

RF coils are used both for exciting the spins and for receiving signal from the spins. Regarding the use of RF coils to receive signal, the smaller the coil, the less tissue to which it couples. This gives a higher signal-to-noise ratio but results in less brain coverage. Larger RF coils allow for more brain coverage but have a lower signal-to-noise ratio than smaller coils. Where sensitivity is critical, a surface coil in a specific region may be desirable. A brain-specific RF coil should be generally as close to the head as possible so that it couples only to brain tissue. Where whole brain imaging is required, a whole brain quadrature RF coil is likely to be optimal. It should be noted here that typical whole *head and neck* coils used clinically are sub optimal for whole brain fMRI, since they couple also to the face and neck regions (only adding noise), and they are generally not as close as possible to the head.

Regarding the use of RF coils for excitation, the larger the coil the more uniform the excitation distribution. This is desirable for maintaining uniform contrast. Obtaining uniform excitation with a small coil usually requires the use of specialized RF pulses. Thus, the optimal solution is to use a large RF coil for excitation of the spins, and a separate smaller coil for signal reception. When multiple RF receiver channels are available with the appropriate bandwidth for high speed imaging, multiple smaller RF coils can be used simultaneously as receive coils and a larger coil for excitation. In this manner, the advantages of each coil size are combined.

At high field strengths, because of RF power deposition issues, it has been difficult to use whole body

RF coils for excitation. Currently at field strengths of 3 Tesla and above, excitation coils are limited to brain RF coils.

Voxel size

The signal-to-noise ratio in an MR image is directly proportional to voxel volume. Functional contrast-to-noise ratio is optimized by matching the volume of the active region to the voxel volume. This matching of voxel volume to activated region minimizes the partial volume averaging of inactive tissue while maximizing the signal-to-noise ratio. Since functional region sizes are not well characterized, and are likely to vary widely over space and across experimental question, the optimal voxel size is difficult to predict. Recent work suggests that the optimal voxel volume dimensions are $1.5 \times 1.5 \times 1.5$ mm^3 (Hyde *et al.* 2000). Matching the voxel volume to the cortical thickness—about 3 mm—is also a common practice. The issue becomes more complicated when one takes into consideration physiological noise, which is nearly independent of voxel volume. More work must be done to characterize this.

One other advantage to imaging with smaller voxels is that, particularly in regions of poor shim, T2* tends to increase as voxel volume is reduced, providing higher signal at a given TE and, subsequently, more functional contrast (see also Chapter 4). Because the voxel size dependence is so much dependent on the shim, the precise relationship between voxel size and T2* cannot be simply predicted. Methods for decreasing the voxel volume include using a longer readout window with more points, using partial *k*-space reconstruction techniques, and using multi-shot techniques – all are discussed in Section 6.4.

6.3.3 Reducing physiological fluctuations

In most fMRI studies which use snap shot imaging, a large contribution to the temporal stability of the images over the time scale of min, as opposed to the typical 30 ms acquisition time per snap shot image, is from physiological processes. The brain pulsates with every heart beat (Poncelet *et al.* 1992; Dagli *et al.* 1999). Also, the effect of the lungs filling with air with every breath changes the magnetic field profile passing through the brain. This change in magnetic field profile causes changes in image placement and geometry. Breathing also modulates the cardiac frequency. Additionally, physiological fluctuations in the 0.1 to 0.2 Hz range have been observed in MRI data. Some have attributed these low frequency oscillations to vasomotion (Mayhew *et al.* 1996). Others have attributed them to spontaneous brain activity (Biswal *et al.* 1995; Lowe *et al.* 1998). Aside from the fact that they are interesting in themselves, these physiological fluctuations, when not the topic of study, should be removed to reap full sensitivity. These fluctuations are less of a hindrance at extremely high spatial resolution or when using a pulse sequence with a low contrast sensitivity, in which case random thermal noise effects are similar in magnitude to the physiological fluctuations, and tend to dominate.

Filtering

Filtering out frequencies associated physiological processes can reduce the temporal fluctuations or at least make their noise contribution closer to a Gaussian distribution so that standard parametric statistical tests can be applied. Filtering is also a relatively easy post-processing step. It should be noted that if the frequencies do not overlap with the frequency spectrum of the haemodynamic impulse response function, then they are inconsequential to the data quality and do not need removing, particularly when performing regression or correlation analysis with a realistic reference function that contains all the frequencies that are of interest.

One major difficulty in filtering out the effects of physiological processes from the MRI data itself is that it is necessary to sample the processes at a rate at least double that of the highest fluctuation frequency in order to remove them. To properly filter cardiac frequencies, for example, it is required that the scan TR be very short since the frequencies of fluctuations induced by the cardiac cycle can be much higher than the heart rate itself. Because the sampling rate for most fMRI studies is typically in the range of 2 s per sampling of the same slice, the cardiac frequencies typically cannot be removed by analysis of the MRI data alone. Strategies have been used, with limited results, to work around this undersampling problem (Frank *et al.* 1999; Lowe 1999).

Filtering of respiration related fluctuations is easier since the respiration frequency is well within the sampling rate of most time series. One method for filtering involves applying to the data a band-stop filter in the range of the respiration frequencies. Another method, which is generally more accurate, involves using the respiration time course, obtained from direct measurement using a billows in the scanner, as a regressor or reference function in data analysis. This function can then be subtracted out of or orthogonalized to the data. The regions that appear the most affected by respiration are similar to those most affected by cardiac fluctuations—typically at the base of the brain.

Pulse sequence strategies

Standard multi-shot techniques suffer from significantly more physiological-related noise than do EPI techniques or single and multi-shot spiral imaging (Glover and Lee 1995; Noll *et al. 1995*). This is because standard multi-shot images take several s to acquire, during which time physiological processes evolve, introducing 'ghosting' into the images. The magnitude of the ghosts in single and multi-shot imaging depends on how well individual lines of *k*-space are registered. With multi-shot imaging the *k*-space lines are acquired over, say, 3 s. The relative phase of each *k*-space line (or its 'placement') is particularly dependent on when in the cardiac cycle it is collected, so one can imagine that no multi-shot image will have precise placement of *k*-space lines due to the non-repeatability of the phase of the cardiac cycle relative to the timing of data collection. This leads to non-repeatable ghosting which adds an order of magnitude more temporal instability to the time series. The lines near the centre of *k*-space contribute most to the image intensity, so it is primarily important to have those lines registered across all images. Multi-shot *spiral* techniques perform better since they always start data acquisition at the centre of *k*-space, therefore oversampling this region. Manifestation of any differences in the phase of the cardiac cycle near the centre of *k*-space tends to get reduced with multi-shot spiral techniques because of this oversampling. Regardless, multi-shot techniques should generally be used only if extremely high resolution is desired (Menon and Goodyear 1999) either for imaging small activated regions or for minimizing signal dropout. Unwanted fluctuations associated with single shot imaging are much more readily corrected than those associated with multi-shot techniques.

For snap shot EPI, each image is essentially captured in 30 to 40 ms, 'freezing' any physiological process and making each line within an individual image consistently 'registered' relative to all other lines. Ghosting may occur, but it does not significantly fluctuate over time.

Another solution to the instability problem of multi-shot techniques is the application of navigator pulses or retrospective correction (Stenger *et al.* 1999; Hu and Kim 1994; Glover and Lai 1998). Navigator pulses can also be useful for correction of head motion when using single shot techniques (Lee *et al.* 1996).

While discussing ghosting, it is worth mentioning that ghosts from blood vessels are also created, due to fluctuations in the flow velocity. With EPI, one can see these as small ghosting variations propagating from the vessel in the phase encode direction as the blood velocity changes with the cardiac cycle between images. These are easily recognized as a small smear of artefact in one direction, with spiral sequences the artefact appears differently. Because of the way in which single-shot spiral scans are collected (centre-out in *k*-space as opposed to bottom-up or top-down), the vessel ghost is no longer a linear smear, but instead is a ripple in all directions, which can be more problematic for functional imaging near these pulsatile vessels since this ripple causes changes throughout the brain.

Finally, while gradient echo and asymmetric spin echo techniques have similar contrast weightings, asymmetric spin echo sequences are somewhat less sensitive to rapidly flowing blood and to the artefacts induced by changes in the velocity of rapidly flowing blood (Baker *et al.* 1993). The reason for this is that asymmetric spin echo sequences involve the application of two RF pulses: the 90° excitation pulse and then, about 40 ms later, a 180° refocusing pulse. Rapidly flowing blood that has experienced the initial 90° pulse has mostly flowed out of the imaging plane by the time that the 180° pulse is applied, therefore not contributing to the signal. With a gradient echo sequence, only the excitation pulse is applied, therefore including this rapidly flowing and pulsatile blood.

Gating

Gating of the data acquisition to the cardiac cycle would seem to be a simple solution to the problems of cardiac-induced signal fluctuation. However, the technique presents a serious drawback. Gating involves triggering of the scanner to the heart beat so that an image is always collected at a specific phase of the cardiac cycle. This is advantageous because a primary source of physiological noise is the collection of images at varying phases of the cardiac cycle causing head misregistration (the brain moves with every heart beat) and pulsatile flow artefacts. Image collection at a single cardiac phase would eliminate this misregistration, thereby reducing the noise and potentially increasing the spatial resolution of fMRI (i.e. the brain would be imaged at a single position for every acquisition). The drawback to gating is that if the heart rate changes during the collection of images, the MR signal intensity also changes, depending on the tissue T1 and the average TR used. This generally causes even larger fluctuations in the data—making gating relatively worthless in the context of fMRI. A technique has recently been developed to correct the global fluctuations that occur with changes in heart rate, therefore making gating a feasible option in fMRI (Guimaraes *et al.* 1995; Guimaraes *et al.* 1998). Gating would be especially useful for identifying activation in structures at the base of the brain since that is where pulsatile motion is greatest, where activation is most subtle, and where activated regions are the smallest—requiring the most consistent image to image registration.

Cardiac gating and subsequent T1 correction is cumbersome to implement. A precise record of the timing of each heart beat must be maintained and used in the correction. Also, the TR is variable, which leads to more difficulty in properly binning the data relative to the brain activation timing. In addition, the minimum TR is limited to the average cardiac cycle. One unique advantage to this technique is that a map of T1 can be derived from the correction data at no additional cost, perhaps useful for subsequent cortical parcellation. Also, gating is the only means by which it is certain that the tissue content in each voxel will remain constant. This may be critical when imaging small structures at the base of the brain.

6.3.4 Minimizing temporal artefacts

Temporal artefacts are less cyclic signal changes introduced into the time series by means other than physiological fluctuations (which are thought of here as being more cyclic). Temporal artefacts can be caused by, among other things, scanner instabilities and subject motion. The methods for reducing sensitivity to these effects are described below.

Brain activation paradigm timing

The choice in fMRI timing is usually determined by the sluggishness of the haemodynamic response (it is usually not useful to go much faster than an on-off cycle of 8 s on and 8 s off), by the particular brain system that is being activated, and by the predominant frequency in the power spectrum of the noise. As a rule-of-thumb, the goal is to maximize both the number of on–off cycles and the amplitude of the signal response during each cycle in order to optimize the power of the post-processing techniques. This is particularly true when using correlation analysis to extract functional information since much of the artefactual signal change energy (from signal drift or slow motion) is in the lower frequencies. Generally, contrast-to-noise ratio is maximized and artefact is minimized by cycling the activation at the highest rate with which the haemodynamics can keep up and by having a time series no longer than about 3 to 4 min in duration.

A second strategy has recently proven effective for separating activation-induced signal changes from artefact. Activation related to overt word production has been successfully imaged using fMRI (Birn *et al.* 1999), this being previously thought problematic due to head motions during overt speech. The strategy uses the knowledge that the artefactual signal changes associated with moving the jaw have a very different time course than the haemodynamic response of the desired signal changes associated with brain activation. The action of speaking introduces a rapid signal change that lasts only as long as the jaw is out of its resting position. The positive BOLD response to a brief task only begins to increase after 2 s, peaks about 5 s later, and takes an additional 6 s to return to baseline. If an event-related overt word production paradigm is used, the artefactual signal can be easily separated

from the BOLD signal change and removed from the time series.

Post processing

Motion correction methods have been developed for fMRI and are used on a routine basis (Woods *et al.* 1992; Eddy *et al.* 1996; Cox and Jesmanowicz 1999). These have been further refined by methods to correct for non-equilibrium signal induced by through-plane motion (Friston *et al.* 1996). Limits do exist as to how robustly these techniques perform. First, for most fMRI acquisition sequences the slices in the volume are not collected simultaneously, so the assumption of rigid motion cannot be made. Second, motion beyond a few voxels typically causes most of these methods to fail in practice.

Real time fMRI

It is often more efficient to re-collect a poor run rather than spend time trying to perform motion correction and artefact reduction afterwards. This approach is only possible if the anatomical and functional data quality can be monitored as it is collected. Several groups have developed methods by which EPI data are collected, reconstructed, and repeatedly analysed in 'real time', allowing for quality assessment (Cox *et al.* 1995; Cox and Hyde 1997; Cox and Jesmanowicz 1999). In the context of clinical fMRI, this immediate feedback can be critical since the information needs to be correct in one pass. One can also imagine cognitive and other experiments that are iterative in nature, being performed in a branching manner depending on the previously obtained results. In addition, many experiments may require 'tuning' the stimulus quality or slice location to optimize the results. All of these methods would benefit from 'real-time' fMRI.

Physical restraint

Methods of physical restraint of the head to prevent motion include packed foam padding, a simple tape across the nose or forehead for feedback, a bite bar, a head vice, a face mask, and a head-neck cast. All methods used to date have found limited success which depends not only on effectiveness of immobilization but also critically on the motivation and comfort of the volunteer. Even with the most motivated and comfortable volunteer, sub-voxel motion still occurs. In addition, physiological fluctuations—brain, blood, and CSF motion—remain.

Pulse sequence strategies

Many pulse sequence strategies exist for reducing the impact of subject head motion. These include clustered volume acquisition, phase encode direction adjustment, slice orientation adjustment, image contrast manipulation, and the application of crusher gradients.

A novel image collection timing scheme, called clustered volume acquisition, was first introduced by Talavage *et al.* (1998) to alleviate the problem of artefactual auditory activation arising from the scanner noise (Bandettini *et al.* 1998) when performing auditory activation experiments (Melcher *et al.* 1999). Typically with EPI on clinical scanners the individual slice acquisitions are spaced evenly within a TR. For example, if 10 slices are specified with a TR of 2 s, then the acquisition of each slice is spaced 200 ms apart. With clustered volume acquisition, the ten slices are collected as rapidly as possible, followed by a period of silence during the remainder of the TR interval. Since the positive BOLD haemodynamic response lags temporally from the brain activity, it is not necessary to collect images during the immediate time of stimulation. Rather, after waiting a time from 4 to 6 s after auditory stimulation, the imaging gradients may be applied to collect the images without introducing artefactual activation. This technique lends itself well to presenting auditory stimuli without contamination from the 100–130 dB EPI scanner noise. In addition, it lends itself to having subjects give brief overt responses (which might otherwise cause motion artefacts) without any time series contamination. An important further issue in clustered volume acquisition is that for the effects of the scanner noise on the haemodynamic response to be *completely* eliminated there must be a sufficient period of silence to allow for the signal from cortex activated by scanner noise to return to baseline. This will add about 6 s on to the necessary TR, making the scan prohibitively long for many types of experiment.

Some amount of image ghosting invariably exists in EPI images, and these ghosts often overlap with the main image. The ghosts are usually stable over time

and do not contaminate the time series. However, if they vary, as can be the case with subtle eye movements, then instability in the ghost can introduce instability in the main image. A common strategy is to set the phase encoding direction of the EPI acquisition such that the ghosts minimally overlap with brain tissue. In this manner any artefactual signal changes that occur in the ghosts or that cause the ghosts to change slightly will be clearly identified as such since they occur outside the brain.

The motion correction schemes mentioned above benefit substantially from having the entire volume collected as rapidly as possible. The use of clustered volume acquisition, 3D fMRI techniques (Yang *et al.* 1996), and PRESTO (Liu *et al.* 1993; Ramsey *et al.* 1996; Ramsey *et al.* 1998; Golay *et al.* 2000), allow for simultaneous volume acquisition, and are therefore beneficial to motion correction algorithms that assume rigid body motion.

When images in the volume cannot be collected simultaneously, it is through-plane motion that is hardest to correct properly. It is therefore useful to chose the imaging plane along which the most motion is expected to occur. Most head motion during fMRI runs is typically a head-bobbing motion. For this reason, the choice of a sagittal plane for slice collection usually allows for better motion correction results.

Since artefactual signal changes originating from head motion only arise if adjacent voxels have differing signal intensities, a flatter time series image contrast will reduce the effects of small sub-voxel motion. Typically, a flat contrast is achieved with gradient echo (T2*-weighted) EPI using a TR that is less than 2 s.

It has been shown that when using a short TR the existence of magnetization remaining in the transverse plane can enter into the time series during subsequent RF pulses. This results in variably periodic 'stimulated echoes' that add to the temporal instability. Simple application of 'crusher gradients' (a gradient pulse at the end of the TR period lasting for ≈ 10 ms) effectively removes this 'left over' transverse magnetization and increases temporal stability (Zhao *et al.* 2000).

Stimulus equipment

Many stimulus and subject interface devices, such as projectors, joysticks, and button boxes, emit RF noise. If these devices are used in the scanning room or wires from them are passed through wave guides into the magnet room, it is important to make sure that they are properly shielded. Ideally, all wires should pass through a filtered penetration panel. Otherwise, this 'RF noise' can significantly contaminate image temporal stability. One method for checking this is by inspecting the high resolution anatomical images. If these have any prominent stripes passing through them, then there exists RF contamination that should be removed.

6.4 Issues of resolution and speed

The following section considers some of the issues relating to selection of the possible and the optimal temporal resolution and spatial resolution in fMRI experiments. These issues are dealt with in greater detail in Chapter 7.

6.4.1 Acquisition speed

The image acquisition rate is limited ultimately by how rapidly the signal can be digitized by the scanner and by how rapidly the imaging gradients can be switched. As discussed above, MR imaging can be divided into single-shot and multi-shot techniques. In single-shot imaging, spins are excited with a single excitation pulse and all the data necessary for creation of an image are collected at once. Echo planar imaging is the most common single shot technique. (With one echo train an entire image 'plane' is acquired). Multi-shot techniques are the most commonly used method for high resolution anatomical imaging. Usually, a single 'line' (in *k*-space) of raw data is acquired with each excitation pulse. Because of the relatively slow rate at which the magnetization returns to equilibrium following excitation (determined by the T1 of the tissue), a certain amount of time is required between shots, otherwise the signal would rapidly be saturated. Because of this required recovery time (at least 150 ms), multi-shot techniques are typically slower than single shot techniques. For a 150 ms TR, a fully multi-shot image with 128 lines of raw data would take 150ms × 128 = 19.2 s.

In the case of echo-planar imaging, the entire data set for a single plane is typically acquired in about 20

to 40 ms. For a BOLD experiment, the time to echo (TE) is about 40 ms. Along with some additional time for applying other necessary gradients, the total time for an image to be acquired is about 60 to 100 ms, allowing 10 to 16 images to be acquired in a second. Improvements in digital sampling rates and gradient slew rates will allow small further gains in this figure, but essentially this is about the upper limit for imaging humans.

In the context of an fMRI experiment with echo planar imaging, the typical image acquisition rate is determined by how many slices can temporally fit into a TR time. For whole brain imaging, approximately 20 slices (5 mm thickness) are required to cover the entire brain. This would allow a TR of about 1.25 to 2 s at minimum. This sampling rate is more than adequate to capture most of the details of the slow and dispersed haemodynamic response. Even with a relatively long TR or image acquisition rate, the temporal resolution may be improved by spacing the image timing unevenly with the task timing, therefore sampling a different part of each on-off cycle.

6.4.2 Image resolution

The spatial resolution is also primarily determined by the gradient strength, the digitizing rate, and the time available. For multi shot imaging, as high resolution as desired can be achieved if one is willing to wait: one can keep on collecting lines of data with more RF pulses. For snap-shot echo planar imaging, the free induction decay time, T2*, plays a significant role in determining the possible resolution (Jesmanowicz *et al.* 1998). One can only sample for so long before the signal has completely decayed away. For this reason, echo planar images are generally lower resolution than multi-shot images. To circumvent the problem of decaying transverse signal, two strategies are commonly used (Cohen and Weisskoff 1991; Cohen 1999). The first strategy is multi-shot EPI, in which a larger *k*-space data set is acquired in multiple interleaved passes (but still with many fewer passes than for conventional clinical multi-shot imaging). The second strategy is to perform an operation called conjugate synthesis, which involves making use of the fact that due to a symmetry in the full *k*-space data, half of the data that conventionally is collected is redundant. By only measuring the minimum lines required, the uncollected lines of *k*-space can be calculated using the symmetry properties. This allows a gain of at most twice the spatial resolution, with some cost in signal-to-noise ratio and image quality. The procedure is also known as partial *k*-space EPI.

Multi-shot EPI suffers from some of the same temporal stability problems as other multi-shot techniques, mentioned in Section 6.3.4 above. Navigator echoes can be used to effectively correct these *k*-space misregistration problems. With partial *k*-space acquisition, the image quality tends to suffer because complete phase information is not obtained, causing the phase correction accuracy for all lines of *k*-space to be degraded. A further advantage of multi-shot EPI is that if the resolution is kept the same as with single-shot imaging, the effective readout echo intervals are shorter, reducing image distortion.

6.4.3 Brain coverage

All MRI sequences can give full brain coverage. The goal is to achieve the most uniform brain coverage as rapidly as possible. Single shot EPI or spiral sequences can achieve complete brain coverage within 2 s. Many 3D sequences, including PRESTO, are becoming increasingly popular in fMRI applications (Yang *et al.* 1996; Liu *et al.* 1993; Ramsey *et al.* 1996; Golay *et al.* 2000). Other than the temporal resolution and simultaneity issues in regard to brain coverage, a key concern is making sure that specific areas in the brain, such as near the base, orbits, and ear canals, are covered. This issue is discussed in the following section.

6.5 Structural and functional image quality

Even though it is the time series stability that gives the most difficulty, the anatomical image quality, for both EPI time series images and the high resolution structural images on which the functional images are registered, is critical for functional localization.

6.5.1 Functional time series image quality

Image quality issues that are the most prevalent in time series image collection are image warping (Jezzard and Clare 1999) and signal dropout (Glover 1999). While

much can be written on this subject, the description here is kept to the bare essentials.

Image warping or distortion is fundamentally caused by one or both of two things: B_0 field inhomogeneities and gradient non-linearities. A non linear gradient will cause non-linearities in spatial encoding, causing the image to be distorted. This is primarily a problem when using small (e.g. head-only) gradient coils that have a small region of linearity that drops off rapidly at the base and top of the brain (Wong *et al.* 1992). With the growing prevalence of whole body gradient-coils for performing echo planar imaging, this problem is less often a major issue.

If the B_0 field is inhomogeneous, as is typically the situation with imperfect shimming procedures—particularly at higher field strengths—the spins will precess at a different frequency than is expected in their particular location. This leads to image deformation in those areas of poor shim—particularly with an imaging procedure that requires a long readout window (e.g. snap-shot EPI). A solution to this is to shorten the readout window, achieve a better shim (Glover 1999; Constable *et al.* 2000), or map the B_0 field and perform a correction based on this map (Weisskoff and Davis 1992; Jezzard and Balaban 1995).

Another potential solution is the use of a spiral readout window instead of EPI. Because of its radial path through *k*-space, spiral imaging manifests off-resonance effects as radial blurring while EPI manifests off-resonance effects as image warping. Spiral readout windows are also typically shorter in duration and more efficient than corresponding EPI readout windows. So, the user performing single shot imaging for fMRI needs to decide if blurring or warping is less problematic.

Signal dropout in gradient echo acquisitions is also caused by localized B_0 field inhomogeneities, typically at the interfaces of tissues having different magnetic susceptibilities. If, within a voxel, the B_0 inhomogeneities are on a smaller scale than the voxel itself, then instead of the voxel being shifted (causing warping) the spins within the voxel will precess at different frequencies and their varying phases will cancel each other out. Several strategies exist for reducing this problem. One is, again, to shim as well as possible at the desired location. Higher order localized shimming is an automated procedure on many scanners, although a full correction of all inhomogeneities is not possible with the available shim terms. Another method is to reduce the voxel size (increase the resolution), thereby having less of a stratification of frequencies within a voxel and therefore less destructive dephasing. A third method is to choose the slice orientation such that the smallest voxel dimension is orientated perpendicular to the largest B_0 gradient. Since in many studies the slice thickness is greater than the in-plane voxel dimension, the slice dimension should *not* be parallel to the direction of highest intrinsic B_0 gradient. Because of this, many studies are performed using sagittal or coronal slice orientations since a prominent gradient in B_0 is in the inferior-superior direction at the base of the brain.

6.5.2 High resolution structural image quality

A technique that should not be overlooked is the necessity for collection of a high resolution anatomical MRI scan that shows good grey-white discrimination. The primary concerns regarding high resolution anatomical image collection include maximizing signal-to-noise ratio, resolution, and image contrast while minimizing the amount of time it takes to collect an entire high resolution data set.

Some groups have aimed to match the degree of geometric warping induced in the high resolution anatomical scan with that of the functional time series data (Sereno *et al.* 1995; Tootell *et al.* 1996, 1998). This has been performed by using T1-weighted, high resolution, multi-shot EPI techniques which have a similar readout window duration as the functional time series images, therefore matching the degree of warping. The warped high resolution anatomical scan can then be unwarped onto a standard high resolution image. This procedure guarantees that precise functional-anatomical registration is achieved.

Practically, it is important to create the highest quality (high resolution, high grey-white matter contrast, and high signal-to-noise ratio) images in about 10 min. While not necessarily optimal, a typical pulse sequence used for this purpose is a 3D spoiled gradient echo sequence (e.g. 3D-FLASH, 3D-SPGR). Typical spoiled gradient recalled parameters used at 1.5 Tesla are: TE = 5 ms, TR = 10 ms, Flip angle = 15°.

At higher magnetic field strengths, maintaining image quality while keeping acquisition time low is an

ongoing challenge. The main reason for this challenge is that, with an increase in static field strength, grey and white matter T1 times become longer, and T2 times decrease (Jezzard *et al.* 1996). This causes the anatomical contrast to flatten out somewhat and requires some adjustment in the timing parameters. Typical spoiled gradient echo pulse sequences and parameters used at 3.0 Tesla are: TE = 4 ms, TR = 9 ms, Flip angle = 12°.

New pulse sequences for performing high resolution structural imaging are still being developed (Deichmann *et al.* 2000; Norris 2000; Wong *et al.* 2000*a*), and may turn out be critical in enabling more precise automatic image segmentation.

6.6 Conclusion

The breadth of knowledge and experience necessary to practice fMRI well has become overwhelming—even for the expert! This chapter has focussed on providing information that is helpful in choosing the optimal pulse sequence and sequence parameters. Of course, this quickly expands into a multi-variable and multi-level optimization problem—ultimately unsolvable. The overall goal of this chapter was of course not to leave the reader overwhelmed, but to give the reader a practical feel for what is important and what is possible: to decide for themselves what variables are critical, and then figure out what they will have to trade-off to achieve a given goal. The potential solutions to any fMRI paradigm/hardware/pulse sequence problem are many. The details or references to details are presented here to aid the reader in choosing the most satisfying solution. Lastly, it is hoped that a sense of excitement in the possibilities of fMRI has also been conveyed. Functional MRI hardware, the understanding of contrast mechanisms, processing techniques, and neuroscience questions continue to co-evolve at a very high rate.

References

Baker, J.R., Hoppel, B.E., Stern, C.E., Kwong, K.K., Weisskoff, R.M., and Rosen, B.R. (1993). In *Dynamic functional imaging of the complete human cortex using gradient-echo and asymmetric spin-echo echo-planar magnetic resonance imaging*. p. 1400, Proceedings of SMRM 12th Annual Meeting, New York.

Bandettini, P.A. and Won, E.C. (1995). Effects of Biophysical and physiologic parameters on brain activation-induced R2* and R2 changes: simulations using a deterministic diffusion model. *International Journal of Imaging Systems Technology*. **6**, 134–52.

Bandettini, P.A., Wong, E.C., Hinks, R.S., Tikofsky, R.S., and Hyde, J.S. (1992). Time course EPI of human brain function during task activation. *Magnetic Resonance in Medicine*, **25**, 390–7.

Bandettini, P.A., Jesmanowicz, A., Van Kylen, J., Birn, R.M., and Hyde J.S. (1998). Functional MRI of brain activation induced by scanner acoustic noise. *Magnetic Resonance in Medicine*, **39**, 410–6.

Belliveau, J.W., Kennedy, D.N., McKinstry, R.C., Buchbinder, B.R., Weisskoff, R.M., Cohen, M.S., Vevea, J.M., Brady, T.J., and Rosen, B.R. (1991). Functional mapping of the human visual cortex by magnetic resonance imaging. *Science*, **254**, 716–19.

Birn, R.M., Bandettini, P.A., Cox, R.W., and Shaker, R. (1999). Event-related fMRI of tasks involving brief motion. *Human Brain Mapping*, **7**, 106–14.

Biswal, B., Yetkin, F.Z., Haughton, V.M., and Hyde, J.S. (1995). Functional connectivity in the motor cortex of resting human brain using echo-planar MRI. *Magnetic Resonance in Medicine*, **34**, 537–41.

Boxerman, J.L., Bandettini, P.A., Kwong, K.K., Baker, J.R., Davis, T.L., Rosen, B.R., and Weisskoff, R.M. (1995*a*). The intravascular contribution to fMRI signal change: Monte Carlo modeling and diffusion-weighted studies *in vivo*. *Magnetic Resonance in Medicine*, **34**, 4–10.

Boxerman, J.L., Hamberg, L.M., Rosen, B.R., and Weisskoff, R.M. (1995*b*). MR contrast due to intravascular magnetic susceptibility perturbations. *Magnetic Resonance in Medicine*, **34**, 555–66.

Buxton, R.B., Luh, W.M., Wong, E.C., Frank, L.R., and Bandettini, P.A. (1998*a*). In *Diffusion-weighting attenuates the BOLD signal change but not the post-stimulus undershoot*. p. 7, Proceedings ISMRM 6th Annual Meeting, Sydney.

Buxton, R.B., Wong, E.C., and Frank, L.R. (1998*b*). Dynamics of blood flow and oxygenation changes during brain activation: the balloon model. *Magnetic Resonance in Medicine*, **39**, 855–64.

Cohen, M.S. (1999). Echo planar imaging and funcational MRI. In *Functional MRI* (ed. C.T.W. Moonen and P.A. Bandettini), pp.137–48, Springer, London.

Cohen, M.S. and Weisskoff, R.M. (1991). Ultra-fast imaging. *Magnetic Resonance Imaging*, **9**, 1–37.

Constable, R.T., Carpentier, A., Pugh, K., Westerveld, M., Oszunar, Y., and Spencer, D.D. (2000). Investigation of the human hippocampal formation using a randomized event-related paradigm and Z-shimmed functional MRI. *NeuroImage*, **12**, 55–62.

Cox, R.W. and Hyde, J.S. (1997). Software tools for analysis and visualization of fMRI data. *NMR in BioMedicine*, 10, 171–8.

Cox, R.W. and Jesmanowicz, A. (1999). Real-time 3D image registration for funcational MRI. *Magnetic Resonance in Medicine* **42**, 1014–8.

Cox, R.W., Jesmanowicz, A., and Hyde, J.S. (1995). Real-time functional magnetic resonance imaging. *Magnetic Resonance in Medicine* **33**, 230–6.

Dagli, M.S., Ingeholm, J.E., and Haxby, J.V. (1999). Localization of cardiac-induced signal change in fMRI. *NeuroImage*, **7**, 407–15.

Davis, T.L., Kwong, K.K., Weisskoff, R.M., and Rosen, B.R. (1998). Calibrated functional MRI: Mapping the dynamics of oxidative metabolism. *Proceedings of the National Academy of Sciences (USA)*, **95**, 1834–9.

Deichmann, R., Good, C.D., Josephs, O., Ashburner, J., and Turner, R. (2000). Optimization of 3-D MP-RAGE sequences for structural brain imaging. *NeuroImage*, **12**, 112–27.

Detre, J.A., Leigh, J.S., Williams, D.S., and Koretsky, A.P. (1992). Perfusion imaging. *Magnetic Resonance in Medicine*, **23**, 37–45.

Duyn, J.H., Moonen, C.T.W., van Yperen, G.H., de Boer, R.W., and Luyten, P.R. (1994). Inflow versus deoxyhemoglobin effects in BOLD functional MRI using gradient-echoes at, 1.5 T. *NMR in Biomedicine*, **7**, 83–8.

Duyn, J.H., Tan C.X., van der Veen, J.W., van Gelderen, P., Frank, J.A., Ye, F.Q., and Yongbi, M. (2000). In *Perfusion-weighted 'single-trail' fMRI*, p.55, Proceedings of ISMRM 8th Annual Meeting, Denver.

Eddy, W.F., Fitzgerald, M., and Noll, D.C. (1996). Improved image registration by using Fourier interpolation. *Magnetic Resonance in Medicine*, **36**, 923–31.

Edelman, R., Siewert, B., and Darby, D. (1994*a*). Qualitative mapping of cerebral blood flow and functional localization with echo planar MR imaging ans signal targeting with alternating radiofrequency (EPISTAR). *Radiology*, **192**, 1–8.

Edelman, R.R., Sievert, B., Wielopolski, P., Pearlman, J., and Warach, S. (1994*b*). Noninvasive mapping of cerebral perfusion by using EPISTAR MR angiography. *Magnetic Resonance Imaging*, **4(P)** [Abstr.], 68.

Frahm, J., Bruhn, H., Merboldt, K.-D., Hanicke, W., and Math, D. (1992). Dynamic MR imaging of human brain oxygenation during rest and photic stimulation. *Magnetic Resonance Imaging*, **2**, 501–05.

Frank, L.R., Buxton, R.B., and Wong, E.C. (1999). In *Detection of physiological noise fluctuations from undersampled multi-slice fMRI data*. p.277, Proceedings, ISMRM 7th Annual Meeting, Philadelphia.

Friston, K.J., Williams, S., Howard, R., Frackowiak, R.S.J., and Turner, R. (1996). Movement related effects in fMRI time-series. *Magnetic Resonance in Medicine*, **35**, 346–55.

Glover, G.H. (1999). 3D z-shim method for reduction of susceptibility effects in BOLD fMRI. *Magnetic Resonance in Medicine*, **42**, 290–9.

Glover, G.H., and Lai, S. (1998). Self-navigated spiral fMRI: interleaved versus single-shot. *Magnetic Resonance in Medicine*, **39**, 361–8.

Glover, G.H. and Lee, A.T. (1995). Motion artifacts in fMRI: comparison of 2DFT with PR and spiral scan methods. *Magnetic Resonance in Medicine*, **33**, 624–35.

Golay, X., Pruessmann, K.P., Weiger, M., Crelier, G.R., Folker, P.J., Kollias, S.S., and Boesiger, P. (2000). PRESTO-SENSE: an ultrafast whole-brain fMRI technique. *Magnetic Resonance in Medicine*, **43**, 779–86.

Guimaraes, A.R., Baker, J.R., and Weisskoff, R.M. (1995). In *Cardiac-gated functional MRI with T1 correction*, p.798. Proceedings of SMR 3rd Annual Meeting, Nice.

Guimaraes, A.R., Melcher, J.R., Talavage, T.M., Baker, J.R., Ledden, P., Rosen, B.R., Kiang, N.Y., Fullerton, B.C., and Weisskoff, R.M. (1998). Imaging subcortical auditory activity in humans. *Human Brain Mapping*, **6**, 33–41.

Haacke, E.M., Lai, S., Reichenbach, J.R., Kuppusamy, K., Hoogenraad, F.G.C., Takeichi, H., and Lin, W. (1997). *In vivo* measurement of blood oxygen saturation using magnetic resonance imaging: a direct validation of the blood oxygen level-dependent concept in functional brain imaging. *Human Brain Mapping*, **5**, 341–46.

Hoge, R.D., Atkinson, J., Gill, B., Crelier, G.R., Marrett, S., and Pike, G.B. (1999*a*). Investigation of BOLD signal dependence on cerebral blood flow and oxygen consumption: the deoxyhemoglobin dilution model. *Magnetic Resonance in Medicine*, **42**, 849–63.

Hoge, R.D., Atkinson, J., Gill, B., Crelier, G.R., Marrett, S., and Pike, G.B. (1999*b*). Stimulus-dependent BOLD and perfusion dynamics in human V1. *NeuroImage*, **9**, 573–85.

Hu, X. and Kim, S.-G. (1994). Reduction of signal fluctations in functional MRI using navigator echoes. *Magnetic Resonance in Medicine*, **31**, 495–503.

Hyde, J.S., Biswal, B.B., and Jesmanowicz, A. (2000). In *Optimum voxel size in fMRI*, p.240, Proceedings, ISMRM 8th Annual Meeting, Denver.

Jesmanowicz, A., Bandettini, P.A., and Hyde, J.S. (1998). Single-shot half *k*-space high-resolution gradient-recalled EPI for fMRI at 3 Tesla. *Magnetic Resonance in Medicine*, **40**, 754–62.

Jezzard, P. (1999). Physiological noise: strategies for correction. In *Functional MRI* (ed. Moonen, C.T.W. and Bandettini, P.A.), pp.173–81, Springer, Berlin.

Jezzard, P. and Balaban, R.S. (1995). Correction for geometric distortion in echo planar images from B_0 field distortions. *Magnetic Resonance in Medicine*, **34**, 65–73.

Jezzard, P. and Clare, S. (1999). Sources of distortion in functional MRI data. *Human Brain Mapping*, **8**, 80–5.

Jezzard, P., Duewell, S., and Balaban, R.S. (1996). MR relaxation times in human brain: measurement at 4 T. *Radiology*, **199**, 773–9.

Kennan, R.P., Zhong, J., and Gore, J.C. (1994). Intravascular susceptibility contrast mechanisms in tissues. *Magnetic Resonance in Medicine*, **31**, 9–21.

Kim, S.-G. (1995). Quantification of relative cerebral flood flow change by flow-sensitive alternating inversion recovery (FAIR) technique: application to functional mapping. *Magnetic Resonance in Medicine*, **34**, 293–301.

Kim, S.-G. and Ugurbil, K. (1997). Comparison of blood oxygenation and cerebral blood flow effects in fMRI: estimation of relative oxygen consumption change. *Magnetic Resonance in Medicine*, **38**, 59–65.

Kwong, K.K., Belliveau, J.W., Chesler, D.A., Goldberg, I.E., Weisskoff, R.M., Poncelet, B.P., Kennedy, D.N., Hoppel, B.E., Cohen, M.S., Turner, R., Cheng, H.M., Brady, T.J., and Rosen, B.R. (1992). Dynamic magnetic resonance imaging of human brain activity during primary sensory stimulation.

Proceedings of the National Academy of Sciences (USA), **89**, 5675–9.

Kwong, K.K., Chesler, D.A., Weisskoff, R.M., and Rosen, B.R. (1994). In *Perfusion MR imaging*, p.1005, Proceedings, SMR, 2nd Annual Meeting, San Francisco.

Kwong, K.K., Chesler, D.A., Weisskoff, R.M., Donahue, K.M., Davis, T.L., Ostergaard, L., Campbell, T.A., and Rosen, B.R. (1995). MR perfusion studies with T1-weighted echo planar imaging. *Magnetic Resonance in Medicine*, **34**, 878–87.

LeBihan, B. (ed.) (1995). *Diffusion and perfusion magnetic resonance imaging*. Raven Press, New York.

Liu, H.L. and Gao, J.H. (1999). Perfusion-based event-related functional MRI. *Magnetic Resonance in Medicine*, **42**, 1011–3.

Liu, G., Sobering, G., Duyn, J. and Moonen, C.T. (1993). A functional MRI technique combining principles of echo-shifting with a train of observations (PRESTO). *Magnetic Resonance in Medicine*, **30**, 764–8.

Lee, C.C., Jack, C.R. Jr., Grimm, R.C., Rossman, P.J., Felmlee, J.P., Ehman, R.L., and Riederer, S.J. (1996). Real-time adaptive motion correction in functional MRI. *Magnetic Resonance in Medicine*, **36**, 436–44.

Liu, T.T., Luh, W.-M., Wong, E.C., Frank, L.R., and Buxton, R.B. (2000). *A method for dynamic measurement of blood volume with compensation for T2 changes*, p.53. Proceedings, ISMRM 8th Annual Meeting, Denver.

Lowe, M.J., Mock, B.J., and Sorenson, J.A. (1998). Functional connectivity in single and multislice echoplanar imaging using resting-state fluctuations. *NeuroImage*, **7**, 119–32.

Lowe, M.J. (1999). In *Gram-Schmidt orthogonalization to reduce aliased physiologic noise in low sampling rate fMRI*, p.1711, Proceedings, ISMRM 7th Annual Meeting, Philadelphia.

Mayhew, J.E.W., Askew, S., Porrill, J., MaxWestby, G.W., Redgrave, P., Rector, D.M., and Harper, R.M. (1996). Cerebral vasomotion: a 0.1 Hz oscillation in reflected light imaging of neural activity. *NeuroImage*, **4**, 183–93.

Melcher, J.R., Talavage, T.M., and Harms, M.P. (1999). Functional MRI of the auditory system. In *Functional MRI*, (ed. C.T.W. Moonen and P.A. Bandettini), p.393–406, Springer, Berlin.

Menon, R.S. and Goodyear, B.G. (1999). Submillimeter functional localization in human striate cortex using BOLD contrast at 4 Tesla: implications for the vascular point-spread function. *Magnetic Resonance in Medicine*, **41**, 230–5.

Menon, R.S., Ogawa, S., Tank, D.W., and Ugurbil, K. (1993). 4 Tesla gradient recalled echo characteristics of photic stimulation—induced signal changes in the human primary visual cortex. *Magnetic Resonance in Medicine*, **30**, 380–6.

Moonen, C.T.W. and van Gelderen, P. (1999). Optimal Efficiency of 3D and 2D BOLD gradient echo fMRI Methods. In *Functional MRI*, (ed. C.T.W. Moonen and P.A. Bandettini), pp.161–72, Springer, Berlin.

Moonen, C.T.W., van ZIJL P.C.M., Frank, J.A., LeBihan, D. and Becker, E.D. (1990). Functional magnetic resonance imaging in medicine and physiology. *Science*, **250**, 53–61.

Noll, D.C., Cohen, J.D., Meyer, C.H., and Schneider, W. (1995). Spiral k-space MR imaging of cortical activation. *Journal of Magnetic Resonance Imaging*, **5**, 49–56.

Norris, D.G. (2000). Reduced power multislice MDEFT imaging. *Journal of Magnetic Resonance Imaging*, **11**, 445–51.

Ogawa, S. and Lee, T.M. (1992). Functional brain imaging with physiologically sensitive image signals. *Journal of Magnetic Resonance Imaging*, **2**(P)-WIP supplement [Abstr.], S22.

Ogawa, S., Lee, T.M., Kay, A.R., and Tank, D.W. (1990). Brain magnetic resonance imaging with contrast dependent on blood oxygenation. *Proceedings of the National Academy of Sciences (USA)*, **87**, 9868–72.

Ogawa, S., Tank, D.W., Menon, R., Ellermann, J.M., Kim S.-G., Merkle, H., and Ugurbil, K. (1992). Intrinsic signal changes accompanying sensory stimulation: functional brain mapping with magnetic resonance imaging. *Proceedings of the National Academy of Sciences (USA)*, **89**, 5951–55.

Ogawa, S., Menon, R.S., Tank, D.W., Kim, S.-G., Merkle, H., Ellerman, J.M., and Ugurbil, K. (1993). Functional brain mapping by blood oxygenation level—dependent contrast magnetic resonance imaging: a comparison of signal characteristics with a biophysical model. *Biophysical Journal*, **64**, 803–12.

Pauling, L. and Coryell, C.D. (1936). The magnetic properties and structure of hemoglobin, oxyhemoglobin, and carbonmonoxyhemoglobin. *Proceedings of the National Academy of Sciences (USA)*, **22**, 210–16.

Poncelet, B.P., Wdeen, V.J., Weisskoff, R.M., and Cohen, M.S. (1992). Brain parenchyma motion: measurement with cine echo planar MR imaging. *Radiology*, **185**, 645–51.

Ramsey, N.F., Kirkby, B.S., Van Gelderen, P., Berman, K.F., Duyn, J.H., Frank, J.A., Mattay, V.S., Van Horn, J.D., Esposito, G., Moonen, C.T., and Weinberger, D.R. (1996). Functional mapping of human sensorimotor cortex with 3D BOLD 4MRI correlates highly with H2(15)O PET rCBF. *Journal of Cerebral Blood Flow and Metabolism*, **16**, 755–64.

Ramsey, N.F., van den Brink, J.S., van Muiswinkel, A.M., Folkers, P.J., Moonen, C.T., Jansma, J.M., and Kahn, R.S. (1998). Phase navigator correction in 3D fMRI improves detection of brain activation: quantitative assessment with a graded motor activation procedure. *NeuroImage*, **8**, 240–8.

Rosen, B.R., Belliveau, J.W., and Chien, D. (1989). Perfusion imaging by nuclear magnetic resonance. *Magnetic Resonance Quarterly*, **5**, 263–81.

Rosen, B.R., Belliveau, J.W., Aronen, H.J., Kennedy, D., Buchbinder, B.R., Fischman, A., Gruber, M., Glas, J., Weisskoff, R.M., Cohen, M.S., Hochberg, F.H., and Brady, T.J. (1991). Susceptibility contrast imaging of cerebral blood volume: human experience. *Magnetic Resonance in Medicine*, **22**, 293–9.

Sereno, M.I., Dale, A.M., Reppas, J.B., Kwong, K.K., Belliveau, J.W., Brady, T.J., Rosen, B.R., and Tootell, R.B. (1995). Borders of multiple visual areas in humans revealed by functional magnetic resonance imaging. *Science*, **268**, 889–93.

Stenger, V.A., Peltier, S., Boada, F.E., and Noll, D.C. (1999). 3D spiral cardiac/respiratory ordered fMRI data acquisition at 3 Tesla. *Magnetic Resonance in Medicine*, **41**, 983–91.

Talavage, T.M., Edminster, W.B., Ledden, P.J., and Weisskoff, R.M. (1998). Comparison of impact of fMRI sequence acoustics on auditory cortex activation. In *6th Proceedings of*

the International Society of Magnetic Resonance in Medicine, p.1503.

Thulborn, K.R., Waterton, J.C., Matthews, P.M., and Radda, G.K. (1982). Oxygenation dependence of the transverse relaxation time of water protons in whole blood at high field. *Biochemica et Biophysica Acta*, **714**, 265–70.

Tootell, R.B., Dale, A.M., Sereno, M.I., and Malach, R. (1996). New images from human visual cortex. *Trends in Neurosciences*, **19**, 481–9.

Tootell, R.B.H., Hadjikhani, N.K., Vanduffel, W., Liu, A.K., Mendola, J.D., Sereno, M.I., and Dale, A.M. (1998). Functional analysis of primary visual cortex (V1) in humans. *Proceedings of the National Academy of Sciences (USA)*, **95**, 811–17.

Turner, R., LeBihan, D., Moonen, C.T.W., Despres, D., and Frank, J. (1991). Echo-planar time course MRI of cat brain oxygenation changes. *Magnetic Resonance in Medicine*, **22**, 159–66.

Ugurbil, K., Garwood, M., Ellermann, J., Hendrich, K., Hinke, R., Hu, X., Kim, S.-G., Menon, R., Merkle, H., Ogawa, S., and Salmi, R. (1993). Imaging at high magnetic fields: initial experiences at 4 T. *Magnetic Resonance Quarterly*, **9**, 259–77.

van Zijl, P.C.M., Eleff, S.M., Ulatowski, J.A., Oja, J.M.E., Ulug, A.M., Traystman, R.J., and Kauppinen, R.A. (1998). Quantitative assessment of blood flow, blood volume, and blood oxygenation effects in functional magnetic resonance imaging. *Nature Medicine*, **4**, 159–16.

Weisskoff, R.M. and David, T.L. (1992). In *Correcting gross distortion on echo planar images*, p.4515, Proceedings, SMRM, 11th Annual Meeting, Berlin.

Weisskoff, R.M., Boxerman, J.L., Zuo, C.S., and Rosen, B.R. (1993). Endogenous susceptibility contrast: principles of relationship between blood oxygenation and MR signal change. In *Functional MRI of the Brain*, pp.103, Society of Magnetic Resonance in Medicine, Berkeley.

Williams, D.S., Detre, J.A., Leigh, J.S., and Koretsky, A.S. (1992). Magnetic resonance imaging of perfusion using spin-inversion of arterial water. *Proceedings of the National Academy of Sciences (USA)*, **89**, 212–16.

Wong, E.C. (1999). Potential and pitfalls of arterial spin labelling based perfusion imaging techniques for functional MRI. In *Functional MRI*, (ed. C.T.W. Moonen and P.A. Bandettini), p.63–70, Springer, Berlin.

Wong, E.C. and Bandettini, P.A. (1999). Simultaneous acquisition of multiple forms of fMRI contrast. In *Functional MRI* (ed. C.T.W. Moonen and P.A. Bandettini), pp.183–92, Springer, Berlin.

Wong, E.C., Bandettini, P.A. and Hyde, J.S. (1992). In *Echo planar imaging of the human brain using a three-axis local gradient coil*, pp. 105, Proceedings SMRM, 11th Annual Meeting, Berlin.

Wong, E.C., Buxton, R.B., and Frank, L.R. (1997). Implementation of quantitative perfusion imaging techniques for functional brain mapping using pulsed arterial spin labeling. *NMR Biomedicine*, **10**, 237–49.

Wong, E.C., Buxton, R.B., and Frank, L.R. (1998). Quantitative imaging of perfusion using a single subtraction (QUIPSS and QUIPSS II). *Magnetic Resonance in Medicine*, **39**, 702–8.

Wong, E.C., Luh, W.-M., Buxton, R.B., and Frank, L.R. (2000*a*). In *Single slab high resolution 3D whole brain imaging using spiral FSE*, p.683. Proceedings, ISMRM 8th Annual Meeting, Denver.

Wong, E.C., Luh, W.-M., and Liu, T.T. (2000*b*). In *Turbo ASL: arterial spin labeling with higher SNR and temporal resolution*, p.452. Human Brain Mapping Meeting, San Antonio.

Woods, R.P., Cherry, S.R., and Mazziotta, J.C. (1992). Rapid automated algorithm for aligning and reslicing PET images. *Journal of Computer Assisted Tomography*, **115**, 565–87.

Yang, Y., Glover, G.H., van Gelderen, P., Mattay, V.S., Santha, A.K., Sexton, R.H., Ramsey, N.F., Moonen, C.T., Weinberger, D.R., Frank, J.A., and Duyn, J.H. (1996). Fast 3D functional magnetic resonance imaging at, 1.5 T with spiral acquisition. *Magnetic Resonance in Medicine*, **36**, 620–6.

Zhao, X., Bodurka, J., Jesmanowicz, A., and Li, S.-J. (2000). B_0-fluctuation-induced temporal variation in EPI image series due to the disturbance of steady-state free precession (SSFP). *Magnetic Resonance in Medicine*, **44**, 758–65.